Chinese Chemical Letters 37 (2026) 111061

Contents lists available at ScienceDirect

Chinese Chemical Letters

journal homepage: www.elsevier.com/locate/cclet

Engineering a γ-glutamyl transpeptidase-activated fluorogenic probe for quantitative visualization and imaging-guided tumor resection

Meng Zhao[a,b], Yan Chen[a], Chenshuo Zhang[a], Jianan Ding[a], Qiulian Mao[a], Yuqi Zhang[a], Yinjia Gao[a], Yongxiang Bai[a], Laiqing Xie[d], Guohua Fan[c,*], Haibin Shi[a,*]

[a] State Key Laboratory of Radiation Medicine and Protection, School of Radiation Medicine and Protection, and Collaborative Innovation Center of Radiological Medicine of Jiangsu Higher Education Institutions, Soochow University, Suzhou 215123, China
[b] Department of Nuclear Medicine, The Second Affiliated Hospital of Anhui Medical University, Hefei 230601, China
[c] Department of Radiology, The Second Affiliated Hospital of Soochow University, Suzhou 215004, China
[d] Department of Ophthalmology, The Second Affiliated Hospital of Soochow University, Suzhou 215004, China

ARTICLE INFO

Article history:
Received 19 December 2024
Revised 7 March 2025
Accepted 9 March 2025
Available online 10 March 2025

Keywords:
Activatable fluorogenic probe
γ-Glutamyl transpeptidase
Ratiometric photoacoustic imaging
Quantitative visualization
NIR imaging-guided surgery

ABSTRACT

Quantitative visualization of pivotal biomarkers and accurate delineation of tumor lesion boundary are highly significant to assist surgeon precisely resect the tumors and reduce the risk of recurrence. Activatable fluorescent probes hold great promise for intraoperative guidance of tumor surgery with high signal-to-background ratio (SBR). Here, we report a γ-glutamyl transpeptidase (GGT)-activated fluorogenic probe Indol-Glu for quantitative visualization of GGT and fluorescence-guided tumor resection. The fluorescence of Indol-Glu was initially "off" state but was specifically activated by GGT to produce enhanced near-infrared (NIR) fluorescence (~37-fold at 741 nm). It is also accompanied by the formation of self-assemblies in the tumor microenvironment resulting in prolonged retention in tumor tissues, which was demonstrated to be able to apply for NIR imaging-guided surgical resection of GGT-overexpressed luciferase-transfected hepatocellular carcinoma (HCC/Luc) tumor. More notably, taking advantage of the ratiometric photoacoustic signal (PA_{690}/PA_{800}) characteristic of Indol-Glu under the digestion of GGT, quantitative visual assessment of GGT activities in various tumor models was achieved in living mice. We believe that this research work may offer a powerful tool for precise diagnosis and surgical resection of malignant tumors.

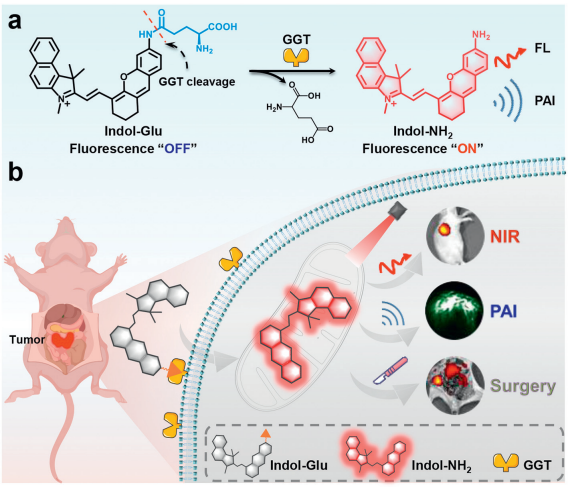
© 2025 Published by Elsevier B.V. on behalf of Chinese Chemical Society and Institute of Materia Medica, Chinese Academy of Medical Sciences.

Early detection and timely surgical resection are very importance to improve the cure rate of patients with malignant tumors [1–3]. The most critical aspects of surgery are to accurately identify and remove the diseased tissue while limiting damage to healthy tissues as much as possible. Positive margins, defined as the presence of residual cancer cells at the margins during surgery, are considered a major cause of local recurrence and poor prognosis [4–6]. This is mainly due to the fact that surgeons highly rely on visual localization and palpation with conventional white light endoscopy, which limits the differentiation between tumor and healthy tissues and increase the risk of tumor recurrence [7,8]. Despite the considerable progress has been achieved in preoperative imaging, such as ultrasound (US), computerized tomography (CT), and magnetic resonance imaging (MRI) etc., the margin positivity rate of solid tumors is still 15%–60% [9–11]. Hence, these imaging modalities do not assist surgeons to accurately identify tumor margins through real-time intraoperative navigation during surgery.

Intraoperative fluorescence imaging has become a very promising tool for accurate delineation of tumor margins and complete surgical resection of tumors due to the advantages of high temporal-spatial resolution, real-time image acquisition, non-invasiveness, portability, and low cost [12–16]. To date, several fluorescent dyes, such as indocyanine green (ICG), methylene blue (MB), and fluorescein sodium, have been approved for clinical utilization [17–23]. However, they still suffer from photo-bleaching, high background noise, and lack of tumor specificity. Activatable fluorescent probes that emit enhanced fluorescent signals only under the action of specific molecular targets or events show great potential in sensitive diagnosis and imaging-guided surgery of tumors because of high signal-to-background ratios (SBRs) and strong specificity [24–30]. Near-infrared (NIR) activatable fluorescent probe holds a great promise for real-time imaging-guided surgical resection as well as postoperative evaluation owing to the deep tissue penetration and low background interference [31–38].

* Corresponding authors.
E-mail addresses: fangh22@sina.com (G. Fan), hbshi@suda.edu.cn (H. Shi).

https://doi.org/10.1016/j.cclet.2025.111061
1001-8417/© 2025 Published by Elsevier B.V. on behalf of Chinese Chemical Society and Institute of Materia Medica, Chinese Academy of Medical Sciences.



Scheme 1. (a) Mechanism of the proposed GGT-mediated hydrolysis of Indol-Glu. (b) Schematic illustration of engineering a γ-glutamyl transpeptidase-activated fluorogenic probe for quantitative visualization and imaging-guided tumor resection.

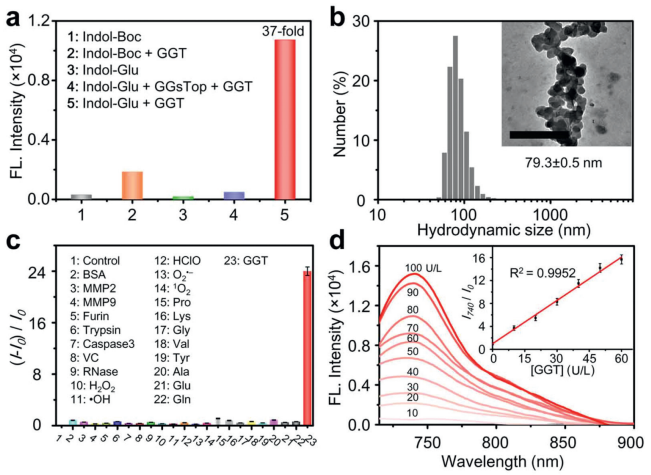


Fig. 1. (a) Fluorescence intensity of Indol-Glu (5 μmol/L) or Indol-Boc (5 μmol/L) in the presence of GGT (100 U/L) with or without GGsTop (0.1 mmol/L). (b) Size distribution profile of Indol-Glu (5 μmol/L) in the presence of GGT (100 U/L) in PBS (10 mmol/L, pH 7.4). The inset is TEM image. Scale bar: 500 nm. (c) Fluorescence intensity ratio $(I-I_0)/I_0$ of Indol-Glu (5 μmol/L) upon addition of various species. (d) Changes in the fluorescence spectra of the Indol-Glu (5 μmol/L) probe with different concentrations of GGT in PBS. The inset is linear fitting curve of Indol-Glu. Data are presented as mean ± standard deviation (SD) ($n = 3$).

Therefore, developing NIR activated fluorescent probes to specifically light up the tumors is of great significance for sensitive detection and precise resection of tumors.

To this end, we herein rationally designed and synthesized a smart molecular probe Indol-Glu that can be specifically recognized and digested by γ-glutamyl transpeptidase (GGT) to emit activated NIR fluorescence for sensitive visualization and imaging-guided resection of tumors. As an important cell surface binding enzyme, GGT plays a crucial role in maintaining cellular homeostasis, but its abnormal expression is closely associated with many diseases such as liver dysfunctions, diabetes, and cancers [39–41]. Probe Indol-Glu was constructed by incorporating the NIR hemicyanine fluorophore with a GGT enzyme-specific peptide. Such amino substitution can efficiently quench the fluorescence of hemicyanine moiety leading to extremely low fluorescence background, whereas the NIR fluorescence signals can be remarkably activated after specific cleavage of hydrophilic γ-glutamyl moiety by GGT accompanied by ratiometric photoacoustic (PA) signals at 690 nm and 800 nm wavelength simultaneously. Meanwhile, the resulting hydrophobic hemicyanine residues tended to self-assemble into uniform nanoparticles, which can potentially enhance the accumulation and retention time of NIR hemicyanine fluorophores in tumors for long-term imaging. More notably, taking advantage of the ratiometric PA signals of Indol-Glu in the presence of GGT, quantitatively visualization evaluation of GGT activities in various tumor models was achieved in living mice (Scheme 1).

The structure of a GGT-activatable NIR fluorescence probe Indol-Glu was rationally designed to include following two components: (i) the enzymatic recognition moiety of γ-glutamyl group that can be specifically cleaved by GGT, (ii) the signaling unit of hemicyanine group that can simultaneously emit activated NIR fluorescence and ratiometric PA signals after enzymatic cleavage. The fluorescence signal of hemicyanine fluorophore is efficiently quenched by the amino substitution of γ-glutamyl group due to the weak intramolecular charge transfer (ICT) [42,43], so the initial fluorescence background of Indol-Glu is extremely low, which is very meaningful for the sensitive detection of species in living system. In brief, γ-glutamyl amino acid was conjugated onto the amino group of hemicyanine fluorophore through the classical amidation reaction to afford Indol-Glu according to previously reported method (Scheme S1 in Supporting information) [44,45]. All compounds including intermediates and Indol-Glu were systematically characterized by nuclear magnetic resonance (NMR) and high resolution mass spectrometry (Figs. S1–S12 in Supporting information).

The absorption and fluorescence spectra of Indol-Glu and the enzymic hydrolytic product Indol-NH_2 (5 μmol/L) were first measured in phosphate buffered saline (PBS, pH 7.4). Indol-Glu showed a strong absorption peak at 587 nm, while the absorption maximum of Indol-NH_2 was located at 689 nm (Fig. S13a in Supporting information). The fluorescence of Indol-Glu is very weak with a quantum yield (Φ) of 0.01%, but Indol-NH_2 emitted intensive NIR fluorescence signals at 741 nm ($\Phi = 3.62\%$, with ICG as the reference) (Fig. S13b in Supporting information), implying that the fluorescence emission of hemicyanine fluorophore was efficiently suppressed by the amino substitution. Further, we also studied the aggregation behavior of Indol-NH_2 in aqueous solution through dynamic light scattering (DLS) and transmission electron microscopy (TEM) measurements. The results clearly indicated that Indol-NH_2 could self-assemble into uniform nanoparticles in aqueous solution with a size of 57.4 ± 0.9 nm, but only a little degree of aggregation (31.7 ± 0.5 nm) was observed for Indol-Glu in aqueous solution indicative of a slightly better water solubility (Fig. S14 in Supporting information), which was further supported by the determination of their absorption variation in DMSO solutions with different volume fractions of water (f_w). With the increase of f_w in solution, the maximum absorption of both Indol-NH_2 and Indol-Glu decreased gradually and blue-shifted to 650–700 nm accompanied by the appearance of another peak shoulder at 644 nm (Fig. S15 in Supporting information), suggesting that both molecules tend to form aggregates in water due to the amphiphilic property.

To investigate the responsibility of Indol-Glu toward GGT, we also synthesized a control probe Indol-Boc in which the carboxyl group was protected by Boc. Indol-Boc is theoretically not response to GGT and cannot be enzymatically cleaved. To verify this, both Indol-Glu and Indol-Boc were treated with the same amount of GGT, respectively. As shown in Fig. 1a, Indol-Glu and Indol-Boc were almost non-fluorescent initially, whereas Indol-Glu showed a dramatic fluorescence enhancement of up to 37-fold upon incubation with GGT. However, no obvious fluorescence enhancement was determined for control Indol-Boc. Interestingly, such fluores-

cence activation of Indol-Glu can be effectively inhibited if the probes were pretreated with an inhibitor of GGT (GGsTop), suggesting that the activated fluorescence signal is attributed to GGT, and Indol-Glu is highly responsive to the GGT, which is also confirmed by the high performance liquid chromatography and high resolution mass spectrometry analysis (Figs. S16 and S17 in Supporting information). Similar to previous TEM results of Indol-NH_2 in aqueous solution, the average size of the resulting nanoparticles after treatment of GGT was determined to be 79.3 ± 0.5 nm (Fig. 1b), again demonstrating that Indol-Glu can be enzymatically digested by GGT. To evaluate the selectivity of Indol-Glu toward GGT, the same amount of Indol-Glu was treated with various species including representative proteases, ROS, amino acids and GGT under the identical condition. As expected, 24-fold fluorescence enhancement was determined only for GGT, but the fluorescence signals of others were quite low (Fig. 1c), indicating that Indol-Glu has a good selectivity toward GGT.

To further examine the detecting sensitivity of Indol-Glu for GGT, Indol-Glu (5 μmol/L) was incubated with various concentrations of GGT ranging from 0 to 100 U/L in PBS (pH 7.4, 37 °C) for 2 h. Fig. 1d evidently shows that the fluorescence intensity of the assays progressively increased and reached a plateau at the concentration of 100 U/L. Notably, the fluorescence enhancements (I_{741}/I_0) of Indol-Glu linearly correlated to the concentrations of GGT in the range of 0–60 U/L ($R^2 = 0.995$). The detection limit was background to be 0.059 U/L (signal-to-noise ratio (S/N) = 3), which is quite similar to other previously reported fluorescence probes, indicative of high sensitivity to GGT. Moreover, the enzyme kinetic parameters of Indol-Glu toward GGT were also calculated by using the Michaelis-Menten equation (Figs. S18 and S19 in Supporting information). The Michaelis constant (K_m) was determined to be 0.70 μmol/L (Fig. S20 in Supporting information), which is much lower than many previously reported probes, suggesting Indol-Glu has strong affinity towards GGT [46–48].

To investigate the fluorescence imaging ability of Indol-Glu to GGT in living cells, its water solubility was first studied by determining the absorption variation of Indol-Glu aqueous solutions at different concentrations. The absorbance of Indol-Glu aqueous solutions increased linearly ($R^2 = 0.99$) with the increasing concentrations (Fig. S21 in Supporting information), indicating that Indol-Glu is water soluble. Methylthiazolyldiphenyl-tetrazolium bromide (MTT) assay results revealed that Indol-Glu had a little effect on the cell viability below 40 μmol/L (Fig. S22 in Supporting information). Besides, standard photon-bleaching experiments demonstrated that it had a good photo-stability under continuous irradiation up to 600 s (Fig. S23 in Supporting information). The blood biochemical analysis results showed that no acute toxicity was observed (Fig. S24 in Supporting information). All these evidences strongly indicate that Indol-Glu possesses a good biocompatibility. To evaluate the responsibility of Indol-Glu toward GGT in living cells, the cell imaging experiments were performed in GGT-positive HCT116 cells as well as GGT-negative NIH/3T3 cells. As illustrated in Fig. 2a, bright NIR fluorescence were detected in Indol-Glu-treated HCT116 cells after 30 min incubation, while almost no fluorescence signals were determined in NIH/3T3 cells under the same condition, suggesting that the fluorescence of Indol-Glu can be activated in cancer cells through the cleavage of γ-glutamyl moiety. Interestingly, the fluorescence mainly located in the cytoplasm rather than the nucleus, which should be due to the fact that GGT mainly locates onto the cell membrane. The proposed mechanism could be attributed to the aggregation of the hydrophobic enzymatic products and activated fluorescence. Moreover, the fluorescence signals could be greatly suppressed when HCT116 cells were pretreated with the inhibitor GGsTop, again demonstrating that Indol-Glu is highly specific for endogenous GGT. Furthermore, flow cytometry analysis results in Fig. 2b clearly show that HCT116 cells

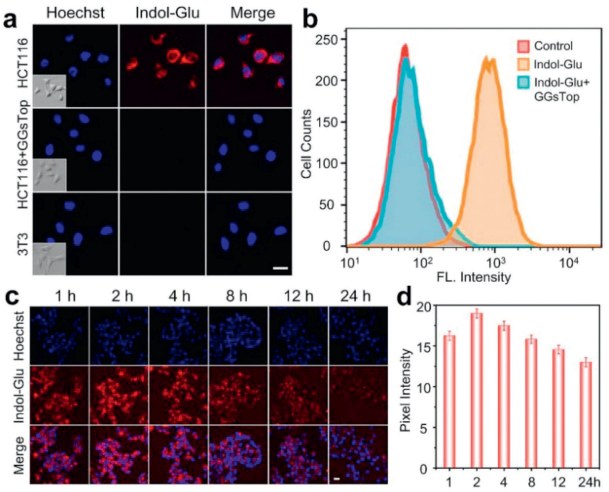


Fig. 2. (a) Fluorescence imaging of 3T3 cells and HCT116 cells incubated with Indol-Glu (5 μmol/L) for 30 min, and HCT116 cells pretreated with GGT inhibitor (GGsTop, 0.1 mmol/L), followed by treatment with Indol-Glu (5 μmol/L) for 30 min. Then, the cells were further treated with Hoechst 33342 for nucleus staining. Scale bar: 20 μm. (b) Flow cytometry analysis of the Indol-Glu incubated in the regular medium and the GGT inhibitor GGsTop pretreated medium for HCT116 cells. (c) Fluorescence imaging of HCT116 cells incubated with Indol-Glu (5 μmol/L) for 30 min then collected at different time points. Scale bar: 20 μm. (d) The quantitative intensity analysis of (c). Data are presented as mean ± SD ($n = 5$).

exhibit the highest shift in the histogram after incubation with Indol-Glu.

To evaluate the intracellular distribution and accurate localization of the resulting fluorescent products, co-locolization experiments were conducted using commercially available dyes Mito or Lyso-Tracker green. The HCT116 cells receiving Indol-Glu exhibited strong NIR fluorescence signals in red color, which overlaid very well with Mito-Tracker green in green color with Pearson's co-localization coefficients of 0.85 (Fig. S25 in Supporting information). These results highly demonstrate that the resulting Indol-NH_2 mainly accumulates in the mitochondria of HCT116 cells owing to its high hydrophobicity. Besides, HCT116 cells were washed and replaced by fresh medium after incubating with Indol-Glu (5 μmol/L) for 30 min, and then imaged by microscopy at selected time points. The results in Fig. 2c indicate that the fluorescence gradually enhanced and reached the maximum at 2 h followed by slow decline. The quantitative analysis indicates that the fluorescence intensity at 24 h was dropped by 34% compared with the intensity maximum (Fig. 2d), suggesting that the probes have prolonged retention time in GGT-positive HCT116 cells. The possible cellular uptake pathway of Indol-Glu was further studied in living cells with respective endocytosis and active transport inhibitors. Highly weak fluorescence signals were actually detected in the cells at 4 °C, and the cells pre-treated with chlorpromazine, an inhibitor for clathrin-mediated endocytosis, showed significantly low fluorescence (Fig. S26 in Supporting information). Together, these results strongly suggest that Indol-Glu enters into HCT116 cells *via* the energy-related clathrin-dependent endocytosis mechanism.

Encouraged by above activated NIR fluorescence of Indol-Glu in cancer cells, we further evaluated its PA signal variation before and after treatment of GGT. The absorption spectra of Indol-Glu before and after incubation with different concentrations of GGT (0–100 U/L) in PBS were measured. With the increasing concentrations of GGT used, the maximum absorbance of Indol-Glu at 584 nm decreased gradually, whereas a shoulder peak at 690 nm increased progressively to maximum concomitant with an isosbestic point at 631 nm (Fig. 3a), which should be due to intensive ICT process.

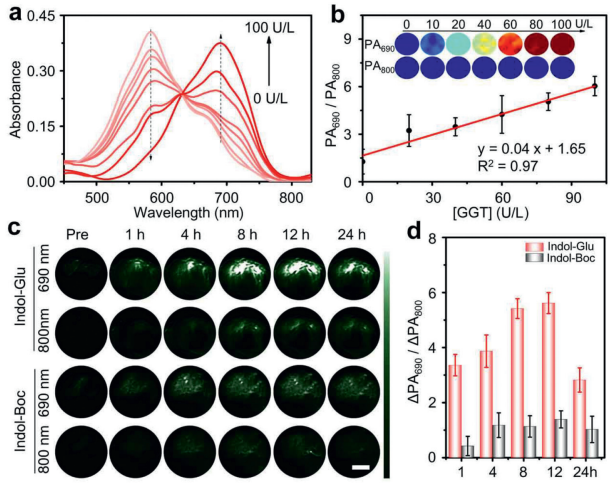


Fig. 3. (a) Changes in the absorption spectra of the Indol-Glu (5 μmol/L) probe with different concentrations of GGT in PBS. (b) Correlation between the PA_{690}/PA_{800} of the Indol-Glu (5 μmol/L) and the concentration of GGT after incubation for 2 h. The inset is PA images of the Indol-Glu solutions containing different amounts of GGT. (c) *In vivo* PA images of HCT116 tumor-bearing mice at various time points (0, 1, 4, 8, 12 and 24 h) after intravenous injection of Indol-Glu and Indol-Boc (100 μmol/L, 200 μL). Scale bar: 2 mm. (d) Quantitative analysis of the $\Delta PA_{690}/\Delta PA_{800}$ intensities of the tumor sites at different time points in (c). Data are presented as mean ± SD ($n = 3$).

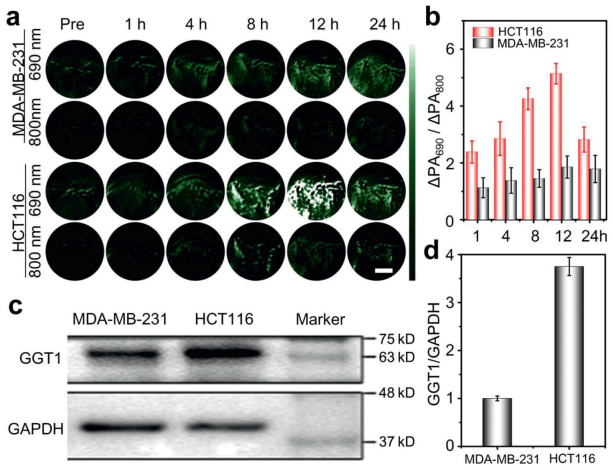


Fig. 4. (a) *In vivo* PA images of MDA-MB-231 and HCT116 tumor-bearing mice at various time points (0, 1, 4, 8, 12 and 24 h) after intravenous injection of Indol-Glu (100 μmol/L, 200 μL). Scale bar: 2 mm. (b) Quantitative analysis of the $\Delta PA_{690}/\Delta PA_{800}$ intensities of the tumor sites at different time points in (a). (c) Western blot assay of the expression level of GGT in MDA-MB-231 and HCT116 tumor-bearing mice at 12 h post-injection of Indol-Glu (100 μmol/L, 200 μL). GAPDH, glyceraldehyde 3-phosphate dehydrogenase. (d) Quantification of the expression level of GGT1/GAPDH in (c). Data are presented as mean ± SD ($n = 3$).

Notably, accompanying the dramatic increase of absorbance at 690 nm, the absorption at 800 nm remains unchanged, which may be useful for quantitative detection of GGT through ratiometric PA assays. We then determined the PA intensity variation of Indol-Glu treated with different amounts of GGT (0–100 U/L) for 2 h in PBS. As expected, the PA intensity at 800 nm (denoted as PA_{800}) remained constant all the time, while the PA signals at 690 nm (denoted as PA_{690}) remarkably enhanced with the increasing concentration of GGT treated (Fig. S27 in Supporting information). The ratiometric PA_{690}/PA_{800} gradually increased from 1.30 to 6.05 with a 4.7-fold enhancement, and the PA_{690}/PA_{800} of Indol-Glu is linearly proportional ($R^2 = 0.97$) to the concentrations of GGT (Fig. 3b). These results reveal that Indol-Glu has a good potential for activated NIR fluorescence imaging of GGT-positive cancer cells as well as quantitative visualization of endogenous GGT through ratiometric PA imaging.

To evaluate the *in vivo* PA imaging performance of Indol-Glu for tumors, the ratiometric PA images upon illumination at 690 and 800 nm were longitudinally recorded by choosing PA_{800} as internal reference after intravenous injection of Indol-Glu or control Indol-Boc (100 μmol/L, 200 μL) into HCT116 tumor-bearing mice. Fig. 3c evidently indicates that the PA signals of tumors at 690 nm progressively enhanced with the increasing time for both probes, while only little PA enhancement at 800 nm was observed. Interestingly, the ratiometric PA_{690}/PA_{800} of Indol-Glu-treated tumor presented a gradual increase and reached the maxima at 12 h post-injection with nearly 4.0-fold enhancement over those treated with Indol-Boc (Fig. 3d and Fig. S28 in Supporting information). Moreover, the PA signals were able to be retained for at least 24 h implying prolonged retention time in tumor tissues. Therefore, these evidences suggest that Indol-Glu can be potentially used for quantitative visualization of GGT *in vivo*. We next employed Indol-Glu to assess the expression levels of GGT in various tumor models. Indol-Glu (5 μmol/L) were incubated with human breast cancer MDA-MB-231 cells and human colorectal carcinoma HCT116 cells for 30 min, respectively. HCT116 cells displayed significantly stronger NIR fluorescence than MDA-MB-231 cells under the same imaging condition (Fig. S29 in Supporting information), indicative of high GGT activity in HCT116 cells.

To quantitatively evaluate the expression of GGT *in vivo*, we established two different subcutaneous tumor models through subcutaneous injection of HCT116 cells or MDA-MB-231 cells into mice. Indol-Glu (100 μmol/L, 200 μL) were intravenously injected into the tumor-bearing mice followed by ratiometric PA imaging. As shown in Figs. 4a and b, the ratiometric PA signals of HCT116 tumor is 2.8-fold higher than that of MDA-MB-231 tumor at 12 h post-injection, again demonstrating that high activity of GGT in HCT116 cells. To further confirm it, the tumors were surgically excised from the mice after intravenous injection of Indol-Glu or Indol-Boc, and the tumorous tissues were then sectioned for fluorescence imaging. Consistently, the tumorous slices of HCT116 showed obviously stronger red fluorescence than MDA-MB-231 (Fig. S30 in Supporting information). Further, western blotting results indicate that the GGT expression in HCT116 tumor is 3.7-fold higher than that in MDA-MB-231 tumor (Figs. 4c and d), which is highly close to the results determined by ratiometric PA imaging. Collectively, these results reveal that our Indol-Glu has a great potential to be used for quantitative visualization of GGT in living system.

Inspired by above promising findings, we next evaluated the capability of Indol-Glu for NIR fluorescence imaging-guided tumor surgery. All animal experiments were conducted according to the Guidelines for the Care and Use of Laboratory Animals of Soochow University and were approved by the Animal Ethics Committee of the Soochow University Laboratory Animal Center (Suzhou, China). After intravenous administration of Indol-Glu, Indol-Boc, or GGT inhibitor + Indol-Glu (100 μmol/L, 50 μL), the subcutaneous HCT116 xenografts tumors were imaged and quantified in a time-dependent manner. Fig. 5a shows that the tumor could be specifically lit up by Indol-Glu, and the NIR fluorescence signals could be efficiently suppressed if the tumor was pre-treated with GGT inhibitor, again supporting that the fluorescence activation of Indol-Glu is highly specific for GGT. In contrast, the decay of fluorescence signals in the Indol-Glu-treated tumor is more than 12 h slower than the ones treated with control Indol-Boc (Fig. 5b), which strongly demonstrates that Indol-Glu has a great prolonged retention effect in tumors.

Encouraged by the high SBR and prolonged retention of our probe within tumors, we further investigated the potential of

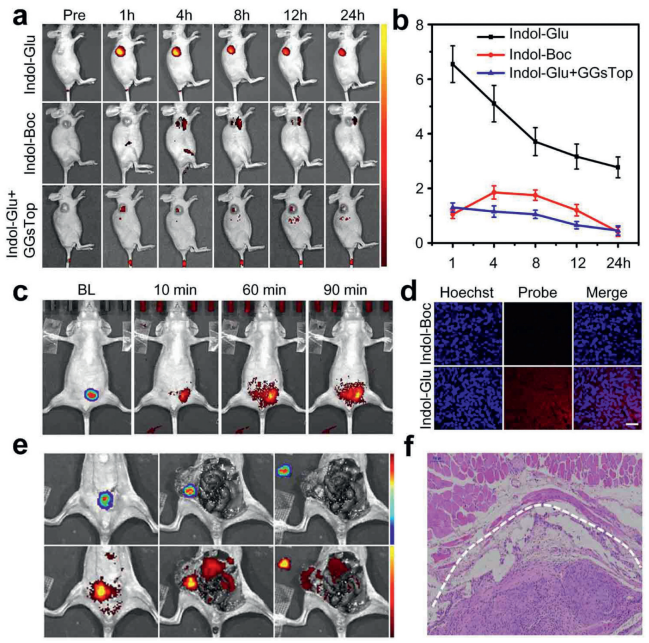


Fig. 5. (a) *In vivo* fluorescence imaging of HCT116 tumor-bearing mice at various time points (0, 1, 4, 8, 12 and 24 h) after intratumoral injection of Indol-Glu and Indol-Boc (100 μmol/L, 50 μL), and HCT116 tumor-bearing mice pre-treated with GGsTop (1 mmol/L, 50 μL) *via* orthotopic injection for 30 min and then intratumorally injected with Indol-Glu (100 μmol/L, 50 μL). (b) Quantitative analysis of the fluorescence intensities of the tumor sites at different time points in (a). (c) *In vivo* fluorescence imaging of HCC/Luc tumor-bearing mice at various time points (10, 60 and 90 min) after intraperitoneal injection of Indol-Glu (100 μmol/L, 200 μL). Bioluminescent images were collected after 10 min of intraperitoneal injection of luciferin (10 mg/mL, 100 μL). (d) Confocal fluorescence microscopy images of tumor tissue slices from HCC/Luc tumor-bearing mice after 1 h intraperitoneal injection of Indol-Glu and Indol-Boc (100 μmol/L, 200 μL). Scale bar: 40 μm. (e) Imaging-guided surgical resection of HCC/Luc tumor-bearing mice after 1 h intraperitoneal injection of Indol-Glu (100 μmol/L, 200 μL). Bioluminescent imaging of mice was used before and after surgery to detect the tumor tissue residuals. (f) Histological HE staining of surgical resection of the tumor in (e). The tumor margins were delineated by white dotted line. Scale bar: 100 μm. Data are presented as mean ± SD ($n = 3$).

Indol-Glu for imaging-guided surgical resection of tumors. For better visualization, the peritoneal luciferase-transfected hepatocellular carcinoma (HCC/Luc) was chosen as a tumor model. The HCC/Luc cells were first incubated with Indol-Glu followed by fluorescence microscopy imaging. As expected, intensive fluorescence was determined in HCC/Luc cells and the fluorescence signals could be completely inhibited by GGsTop (Fig. S31 in Supporting information), implying that GGT is highly expressed in HCC/Luc cells. Next, the HCC/Luc tumor mass (1 mm × 1 mm in size) was inserted into peritoneal space by a midline incision of the abdominal wall under anesthesia to establish the tumor model in mice followed by bioluminescence imaging for tumor growth monitoring. Intensive bioluminescence in abdominal cavity suggested the successful establishment of peritoneal HCC/Luc tumors within a month. After intraperitoneal administration of Indol-Glu (100 μmol/L, 200 μL), strong NIR fluorescence were visualized in the peritoneal cavity of mice at 10 min post-injection, which is consistent well with the bioluminescence imaging region (Fig. 5c). Surprisingly, the fluorescence signals could last for at least 90 min with high T/N ratio, which would be highly helpful for surgical resection of cancerous lesions in clinics. However, the mice with injection of Indol-Boc showed very weak fluorescence in the whole body all the time (Fig. S32 in Supporting information), which is highly consistent with previous *in vitro* experimental results. Moreover, the tumor tissue slices from the mice of Indol-Glu showed remarkably brighter red fluorescence than that of Indol-Boc (Fig. 5d). All these results implies that probe Indol-Glu can be used for accurate diagnosis of tumors *in vivo*.

In light of above promising results, we then performed imaging-guided surgery of peritoneal HCC/Luc tumors after injection of Indol-Glu (100 μmol/L, 200 μL) into the peritoneum. As shown in Fig. 5e, the margin of the tumor was clearly delineated and well distinguished from the surrounding normal tissues. Next, the tumor was thoroughly excised from mice with forceps under the guidance of NIR fluorescence imaging. Meanwhile, the bioluminescence imaging of intraoperative mice confirmed that NIR fluorescence imaging-guided surgery was successfully attempted. Hematoxylin-eosin (HE) staining analysis was also carried out for the surgical tumorous tissues. Fig. 5f showed the characteristics of tumor histology and clear boundary between tumor and normal tissues. Together, these findings strongly demonstrate that Indol-Glu holds a great promise for accurate diagnosis and imaging-guided tumor surgery.

In summary, we have developed a NIR fluorogenic probe Indol-Glu for quantitative imaging of endogenous GGT as well as imaging-guided intraoperative surgery of tumors. The fluorescence of Indol-Glu was "off" state initially, but could be activated by GGT to generate enhanced NIR fluorescence and ratiometric PA signals at 690 nm and 800 nm, allowing for sensitive detection of GGT over-expressed tumors and quantitative visualization of GGT level in living system. Since the hemicyanine residue of Indol-Glu after hydrolysis by GGT is highly hydrophobic, they could self-assemble into uniform nanoparticles in tumor region resulting in prolonged retention time for NIR imaging-guided surgical resection of HCC/Luc tumors. More notably, taking advantage of the ratiometric PA imaging characteristics, Indol-Glu was also employed to quantitatively evaluate the expression levels of GGT in various tumor models in living mice. We thus believe that current study may provide a valuable means for precise diagnosis and surgical resection of malignant tumors.

Declaration of competing interest

The authors declare that they have no known competing financial interests or personal relationships that could have appeared to influence the work reported in this paper.

CRediT authorship contribution statement

Meng Zhao: Writing – original draft, Visualization, Validation, Software, Methodology, Investigation, Formal analysis, Data curation. **Yan Chen:** Visualization, Validation, Investigation, Formal analysis, Data curation. **Chenshuo Zhang:** Methodology, Investigation, Formal analysis, Data curation. **Jianan Ding:** Methodology, Investigation, Formal analysis, Data curation. **Qiulian Mao:** Software, Methodology, Formal analysis. **Yuqi Zhang:** Validation, Software, Methodology. **Yinjia Gao:** Validation, Software, Formal analysis. **Yongxiang Bai:** Writing – review & editing, Visualization, Data curation. **Laiqing Xie:** Software, Resources, Methodology. **Guohua Fan:** Resources, Funding acquisition. **Haibin Shi:** Writing – review & editing, Visualization, Supervision, Resources, Project administration, Funding acquisition, Conceptualization.

Acknowledgments

We acknowledge the financial support from the National Natural Science Foundation of China (Nos. T2325019 and 22077092), Basic Research Program of Jiangsu (No. BK20243030), the special project of "Technological innovation" project of CNNC Medical Industry Co. Ltd (No. ZHYLYB2021001), Four "Batches" Innovation Project of Invigorating Medical through Science and Technology of Shanxi Province (No. 2022XM19), the Open Project Program of the

State Key Laboratory of Radiation Medicine and Protection (Nos. GZK1202309, GZK12023050, GZK12024016, and GZK12024013), and a project funded by the Priority Academic Program Development of Jiangsu Higher Education Institutions.

Supplementary materials

Supplementary material associated with this article can be found, in the online version, at doi:10.1016/j.cclet.2025.111061.

References

[1] D. Crosby, S. Bhatia, K.M. Brindle, et al., Science 375 (2022) 1244.
[2] R. Lawrence, M. Watters, C.R. Davies, et al., Nat. Rev. Clin. Oncol. 20 (2023) 487–500.
[3] J. Phallen, M. Sausen, V. Adleff, et al., Sci. Transl. Med. 9 (2017) eaan2415.
[4] M.S. Moran, S.J. Schnitt, A.E. Giuliano, et al., J. Clin. Oncol. 32 (2014) 1507–1515.
[5] O. Yossepowitch, A. Briganti, J.A. Eastham, et al., Eur. Urol. 65 (2014) 303–313.
[6] P. Ghaneh, J. Kleeff, C.M. Halloran, et al., Ann. Surg. 269 (2019) 520–529.
[7] H. Li, Q. Yao, W. Sun, et al., J. Am. Chem. Soc. 142 (2020) 6381–6389.
[8] Q.J. Duan, Z.Y. Zhao, Y.J. Zhang, et al., Adv. Drug Deliv. Rev. 196 (2023) 114793.
[9] T. Nagaya, Y.A. Nakamura, P.L. Choyke, et al., Front. Oncol. 7 (2017) 314.
[10] K.A. Iczkowski, M.S. Lucia, Prostate Cancer 2011 (2011) 673021.
[11] L. Jiang, S.S. Jiang, H. Long, et al., New Engl. J. Med. 373 (2015) 2186–2188.
[12] J.S.D. Mieog, F.B. Achterberg, A. Zlitni, et al., Nat. Rev. Clin. Oncol. 19 (2021) 9–22.
[13] P. Cheng, K. Pu, Nat. Rev. Mater. 6 (2021) 1095–1113.
[14] S. Hernot, L. van Manen, P. Debie, et al., Lancet Oncol. 20 (2019) e354–e367.
[15] R.R. Zhang, A.B. Schroeder, J.J. Grudzinski, et al., Nat. Rev. Clin. Oncol. 14 (2017) 347–364.
[16] J. Fang, Y. Feng, Y. Zhang, et al., J. Am. Chem. Soc. 144 (2022) 23061–23072.
[17] M. Frumovitz, M. Plante, P.S. Lee, et al., Lancet Oncol. 19 (2018) 1394–1403.
[18] Q.Y. Chen, J.W. Xie, Q. Zhong, et al., JAMA Surg. 155 (2020) 300–311.
[19] Z. Zhou, Y. Liu, W. Song, et al., J. Control. Release 352 (2022) 793–812.
[20] X. Zhao, G. Zhang, J. Chen, et al., Eur. J. Nucl. Med. Mol. Imaging 51 (2024) 1593–1604.
[21] L. van Manen, H.J.M. Handgraaf, M. Diana, et al., J. Surg. Oncol. 118 (2018) 283–300.
[22] J. An, S. Tang, G. Hong, et al., Nat. Commun. 13 (2022) 2225.
[23] X. Chen, J. Sun, J. Mao, et al., Front. Oncol. 13 (2023) 1191470.
[24] M. Gao, F. Yu, C. Lv, et al., Chem. Soc. Rev. 46 (2017) 2237–2271.
[25] C. Wang, Z. Wang, T. Zhao, et al., Biomaterials 157 (2018) 62–75.
[26] X. Shi, Y. Deng, X. Liu, et al., Biosens. Bioelectron. 208 (2022) 114212.
[27] Z. Cheng, Y. Jin, J. Li, et al., J. Nanobiotechnol. 21 (2023) 112.
[28] Y. Yao, S. Chen, C. Yan, et al., Angew. Chem. Int. Ed. 64 (2025) e202416963.
[29] C. Yan, J. Dai, Y. Yao, et al., Nat. Protoc. 18 (2023) 1316–1336.
[30] L. Yin, H. Sun, H. Zhang, et al., J. Am. Chem. Soc. 141 (2019) 3265–3273.
[31] Y. Su, B. Yu, S. Wang, et al., Biomaterials 271 (2021) 120717.
[32] R. Sun, Y. Zhang, Y. Gao, et al., Chem. Sci. 14 (2023) 2369–2378.
[33] S. Zhu, R. Tian, A.L. Antaris, et al., Adv. Mater. 31 (2019) 1900321.
[34] H.D. Li, D. Kim, Q.C. Yao, et al., Angew. Chem. Int. Ed. 60 (2021) 17268–17289.
[35] X. Li, C. Schumann, H.A. Albarqi, et al., Theranostics 8 (2018) 767–784.
[36] Z. Hu, C. Fang, B. Li, et al., Nat. Biomed. Eng. 4 (2019) 259–271.
[37] X. Ni, X. Zhang, X. Duan, et al., Nano Lett. 19 (2018) 318–330.
[38] C. Cui, J. Li, J. Fang, et al., Chin. Chem. Lett. 33 (2022) 3478–3483.
[39] S.K. Kunutsor, Liver Int. 36 (2016) 1723–1734.
[40] A. Fraser, S. Ebrahim, G.D. Smith, et al., Hepatology 46 (2007) 158–165.
[41] K. Takemura, P.G. Board, F. Koga, Antioxidants 10 (2021) 549.
[42] Z.L. Zeng, S.S. Liew, X. Wei, et al., Angew. Chem. Int. Ed. 60 (2021) 26454–26475.
[43] H. Li, H. Kim, F. Xu, et al., Chem. Soc. Rev. 51 (2022) 1795–1835.
[44] Z. Luo, L. Feng, R. An, et al., Chem. Eur. J. 23 (2017) 14778–14785.
[45] Z. Luo, Z. Huang, K. Li, et al., Anal. Chem. 90 (2018) 2875–2883.
[46] P. Zhang, X.F. Jiang, X. Nie, et al., Biomaterials 80 (2016) 46–56.
[47] Z. Hai, J. Wu, L. Wang, et al., Anal. Chem. 89 (2017) 7017–7021.
[48] M. Miao, J. Miao, Y. Zhang, et al., Biosens. Bioelectron. 235 (2023) 115399.